Dynamic soil-structure interaction analysis of a telescope at the Javalambre Astrophysical Observatory

Stijn François[a,*], Pedro Galvín[b], Pedro Museros[c,d], Geert Lombaert[a], Geert Degrande[a]

[a] *KU Leuven, Department of Civil Engineering, Kasteelpark Arenberg 40, B-3001 Leuven, Belgium*
[b] *Universidad de Sevilla, Escuela Técnica Superior de Ingeniería, Camino de los Descubrimientos, 41092 Sevilla, Spain*
[c] *Universitat Politécnica de Valencia, Departamento de Mecánica de Medios Continuos y Teoría de Estructuras, 46022 Valencia, Spain*
[d] *Fundación Caminos de Hierro para la Investigación y la Ingeniería Ferroviaria, C/Serrano 160, 28002 Madrid, Spain*

Abstract

This paper presents the dynamic soil-structure analysis of the main telescope T250 of the Observatorio Astrofísico de Javalambre (OAJ, Javalambre Astrophysical Observatory) on the Pico del Buitre. Vibration control has been of prime concern in the design, since astrophysical observations may be hindered by mechanical vibration of optical equipment due to wind loading. The telescope manufacturer therefore has imposed a minimal natural frequency of 10 Hz for the supporting telescope pier. Dynamic soil-structure interaction may significantly influence the lowest natural frequency of a massive construction as a telescope pier. The structure clamped at its base has a resonance frequency of 14.3 Hz. A coupled finite element - boundary element (FE-BE) model of the telescope pier that accounts for the dynamic interaction of the piled foundation and the soil predicts a resonance frequency of 11.2 Hz, demonstrating the significant effect of dynamic soil-structure interaction. It is further investigated to what extent the coupled FE-BE model can be simplified in order to reduce computation time. The assumption of a rigid pile cap allows to account for dynamic soil-structure interaction in a simplified way. A coupled FE-BE analysis with a rigid pile cap predicts a resonance frequency of 11.7 Hz, demonstrating a minor effect of the pile cap flexibility on the resonance frequency of the telescope pier. The use of an analytical model for the pile group results in an overestimation of the dynamic soil stiffness. This error is due to the large difference between the actual geometry and the square pile cap model for which the parameters have been tuned.

Keywords: Dynamic soil-structure interaction, FE-BE modelling, vibration of sensitive equipment

1. Introduction

The Observatorio Astrofísico de Javalambre (OAJ, Javalambre Astrophysical Observatory) is currently under construction on the Pico del Buitre in the Sierra de Javalambre (Teruel province, Spain). It consists of a large etendue main telescope T250 with 2.5 m aperture and a 3º field of view and an auxiliary T80 JAST (Javalambre Auxiliary Survey Telescope) telescope with 0.80 m aperture and a 2º field of view [1, 2]. The telescopes at the OAJ have been equiped with adaptive optics, a sophisticated technology used in contemporary large ground based telescopes that drastically reduces the effect of wavefront distortion due to atmospheric turbulence through error compensation with deformable mirrors [3, 4]. In order to further improve the quality of the observations, other sources of perturbation have to be mitigated. Vibrations of instruments and the telescope structure are therefore becoming increasingly important [5]. These vibrations are of various origin, such as wind loading and auxiliary mechanical instrumentation (cooler fans, motors,...).

*Corresponding author. Phone: + 32 16 32 16 68. Fax: + 32 16 32 19 88.
Email address: stijn.francois@bwk.kuleuven.be (Stijn François)

Preprint submitted to Soil Dynamics and Earthquake Engineering
Published version: http://dx.doi.org/10.1016/j.soildyn.2014.06.014

Although the site at Pico del Buitre has been selected for its relatively low wind speeds [6, 7], the wind load is still expected to be a major source of vibration. Wind induced buffeting of the telescope structure and turbulence inside the telescope dome are commonly taken into account in the design [8]. Wind loads act on the telescope through the main and secondary mirror and the supporting structure. Wind loads on the exterior of the dome could also be transmitted through the telescope pier [9], although these vibrations are expected to be of minor importance.

The response of the telescope due to the wind loading is governed by lowest the structural eigenmode. As an outcome of the design process of the main T250 telescope, the telescope manufacturer AMOS (Advanced Mechanical and Optical Systems) has imposed that the first resonance frequency of the telescope pier (including the telescope) should be higher than 10 Hz.

Since the telescope pier is a massive construction, it is expected that dynamic interaction between the soil and the telescope pier strongly influences the first resonance frequency [10, 11]. This paper reports on the influence of dynamic soil-structure interaction on the first resonance frequency of the telescope pier. Hereto, a coupled finite element – boundary element (FE–BE) method is employed, in which the FE method allows to model a structure with a complex geometry (the telescope pier founded on a group of reinforced concrete micro-piles) while the BE method enables accounting for the radiation of waves in the soil. The complementarity of both methods is commonly exploited for dynamic soil-structure interaction problems in the time [12–14] or in the frequency domain [15]. In the present analysis, the wind loading results in very small amplitude vibrations that justify a linear approximation. A frequency domain approach is therefore followed. As coupled FE-BE models are computationally expensive [16], it is also investigated to what extent the model can be simplified through the use of approximate foundation impedance functions for pile groups. A simplified model composed of masses, springs and dampers, for which the parameters have been tuned against coupled FE-BE calculations for a large number of floating and end-bearing pile groups [17], is used for this purpose. The accuracy and efficiency of this technique is investigated.

The paper is organized as follows: in section 2, the dynamic soil characteristics at the site of the OAJ are studied by means of two down-hole tests and compared to the results of a geotechnical site survey. The geometry and material properties of the main telescope pier are discussed in section 3. In section 4, the FE model of the telescope pier founded on the pile group is constructed and coupled to a BE model of the surrounding soil. The BE model is verified with a reference solution of the Green's functions of the layered halfspace in section 5. Furthermore, the performance of the proposed model is validated by means of in situ measurements of the pile head impedance. In section 6, the effect of dynamic soil-structure interaction on the dynamic behavior of the telescope pier is studied. Furthermore, it is investigated to what extent the FE-BE model can be simplified in order to reduce computation time.

2. Geophysical site characterization

The OAJ is located at the top of the Pico del Buitre in the Sierra de Javalambre, 1957 m above sea level, close to the village of Arcos de las Salinas (Teruel province, Spain).

An extensive geophysical survey has been carried out [18]. This has revealed a top layer of highly fractured gray bioclastic limestones with a thickness of about 5 m, as shown on the geological section in figure 1. At a depth between 5 m and 7 m, the soil consists of moderately fractured ocher sandy limestones, followed by shales and weakly karstified yellow limestone at a depth between 7 m and 8 m and very porous but resistant red sandy limestone at a depth between 8 m and 9.5 m. The deeper soil layers (from 9.5 m to 22 m) consist of gray calcareous limestone that is slightly fractured and highly resistant.

At the location of the principal dome, the geophysical survey revealed a low stiffness in the top 7 m to 9 m and a low electrical resistivity, which indicates a high porosity as a result of intense ground fracturing. At the location of the minor dome, a significantly higher stiffness and electrical resistivity have been observed.

The shear wave velocity C_s and dilatational wave velocity C_p have been determined from two down hole tests (table 1 and 2). Down hole test 1 has been performed at the location of the minor dome of the T80 telescope, while down hole test 2 has been carried out at the location of the principal dome of the T250 telescope (figure 1). Both down hole tests have been executed prior to excavation of the soft top layers and

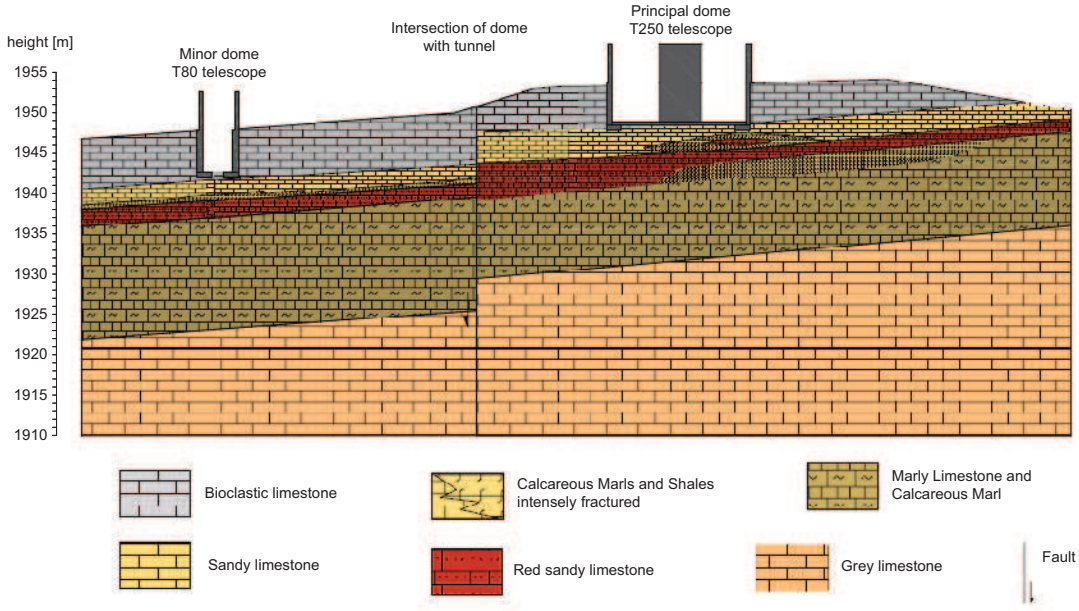

Figure 1: Geological cross section at the construction site [18].

show an increasing soil stiffness with depth. The intense fracturing of the top rock matrix results in low wave speeds in the top layers.

Altitude [m]	Depth [m]	C_s [m]	C_p [m]	ρ [kg/m^3]
1946	1	901	2222	2700
1945	2	685	1852	2700
1944	3	662	1250	2700
1943	4	775	2000	2670
1942	5	820	1539	2670
1941	6	833	2564	2250
1940	7	952	1471	2250
1939	8	901	2083	2250
1938	9	1064	1471	2250
1937	10	1199	2080	2250
1936	11	1109	2753	2650
1935	12	1517	3471	2650
1934	13	1344	2603	2650
1933	14	1458	1870	2650
1932	15	1840	4006	2650
1931	16	2419	3369	2650
1930	17	2595	3945	2650
1929	18	1907	3550	2650
1928	19	1441	2468	2650
1927	20	1928	3022	2650
1926	21	2802	3813	2650
1925	22	2912	4833	2650

Table 1: Dynamic soil characteristics obtained from down hole test 1, prior to excavation.

Altitude [m]	Depth [m]	C_s [m]	C_p [m]	ρ [kg/m^3]
1954	1	408	647	2700
1953	2	403	904	2700
1952	3	446	938	2700
1951	4	490	815	2670
1950	5	521	938	2670
1949	6	521	1191	2250
1948	7	556	1230	2250
1947	8	974	3125	2250
1946	9	1056	3409	2250
1945	10	962	1812	2250
1944	11	1100	2336	2650
1943	12	1064	2670	2650
1942	13	2056	3335	2650
1941	14	1765	2647	2650
1940	15	2150	3164	2650
1939	16	2295	3760	2650
1938	17	1630	3506	2650
1937	18	1383	2635	2650

Table 2: Dynamic soil characteristics obtained from down hole test 2. The properties of the excavated top layers are shown in grey.

The soil is assumed to be horizontally layered, since this allows to use the direct stiffness method [19, 20] for the computation of Green's functions in the BE formulation. Prior to the construction of the telescope, the soft and fractured soil layers up to a depth of 5 m have been excavated as to provide sufficient bearing capacity for the telescope dome. Therefore, results for the first 5 m from down hole test 2 (table 2, prior to excavation) are not considered in the layered halfspace model. The dynamic soil characteristics of the layered halfspace model are plotted in figure 2, where the properties of the layers correspond to layers 6 to 18 of the down hole test in table 2. The underlying homogeneous halfspace is assumed to have a shear wave velocity $C_\mathrm{s} = 2000\,\mathrm{m/s}$, a dilatational wave velocity $C_\mathrm{p} = 3650\,\mathrm{m/s}$, and a density $\rho = 2650\,\mathrm{kg/m^3}$, corresponding to average values from down hole test 2 at larger depths.

The material damping ratios β_s and β_p of the soil define the dissipation of energy in the soil's solid skeleton. Applying the correspondance principle, these ratios determine the imaginary part of the elastic shear modulus $\mu^\star = \mu(1+2\beta_\mathrm{s}i)$ and the constrained or longitudinal modulus $(\lambda+2\mu)^\star = (\lambda+2\mu)(1+2\beta_\mathrm{p}i)$. As the material damping ratio as a function of depth could not be obtained from the down hole tests, an identical value $\beta_\mathrm{s} = \beta_\mathrm{p} = 0.01$ for shear and volumetric deformation is assumed in the following. This low value is not expected to significantly influence the dynamic soil stiffness of the foundation, for which radiation damping rather than material damping is expected to be the dominant mechanism of energy dissipation.

The wave propagation in the layered halfspace (figure 3) is governed by Rayleigh waves. Due to the stratification of the soil, the phase velocity of the surface waves is a function of frequency, described by a dispersion relation [21]. Figure 4 shows the frequency - phase velocity spectrum $\tilde{v}_z(C_r, \omega)$ of the vertical velocity at the free surface of the layered halfspace due to a vertical point load applied at the surface. The spectrum is based on the transformation $\tilde{v}_z(k_r, \omega)$ of the vertical velocity $v_z(r, t)$ to the frequency-wavenumber domain, shown here in terms of the phase velocity $C_r = \omega/k_r$ instead of the wavenumber k_r. The vertical velocity $\tilde{v}_z(C_r, \omega)$ is composed of plane waves with different frequency and phase velocity. Maxima of $\tilde{v}_z(C_r, \omega)$ correspond to the dominant surface waves in the layered halfspace. Three dispersion curves of the layered halfspace are also shown on figure 4. From the first dispersion curve $C_\mathrm{R}(f)$, the Rayleigh wavelength $\lambda_\mathrm{R}(f)$ at the desired first resonance frequency of the telescope $f = 10\,\mathrm{Hz}$ is estimated as $C_\mathrm{R}(f)/f \approx 200\,\mathrm{m}$. The corresponding penetration depth of the Rayleigh waves is estimated as $\lambda_\mathrm{R}/4 = 50\,\mathrm{m}$. This large wavelength at 10 Hz demonstrates that the assumption of a horizontally layered halfspace is

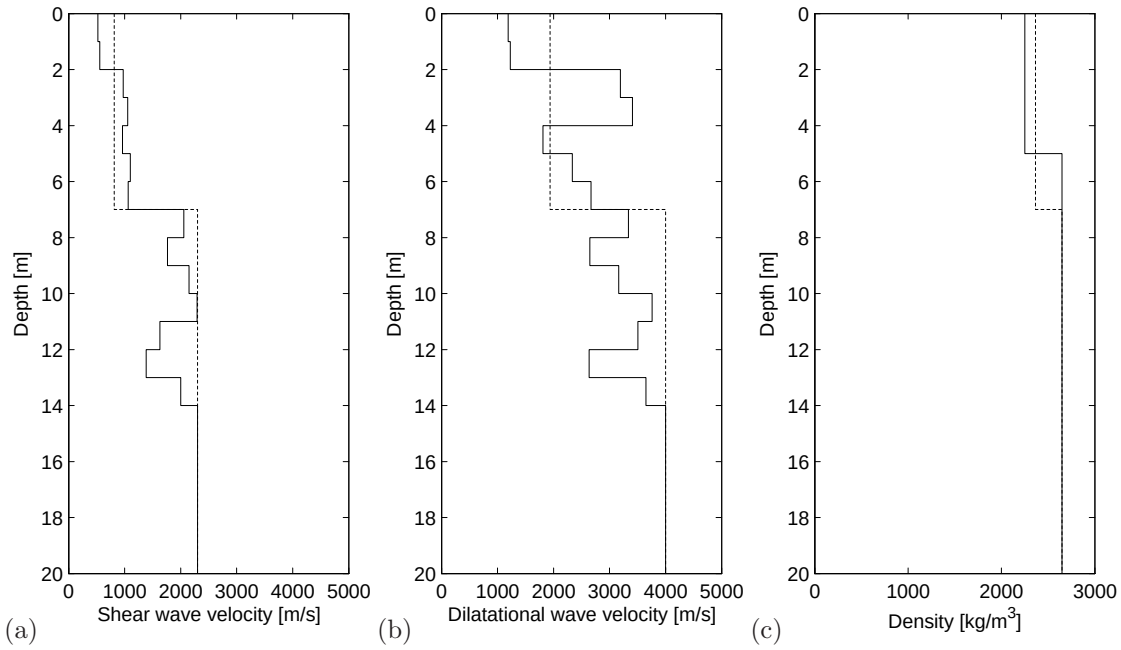

Figure 2: (a) Shear wave velocity, (b) dilatational wave velocity, and (c) density profile determined from the down-hole test after excavation of soft and fractured soil layers upto a depth of 5 m. An equivalent model of a layer on a halfspace, used in the simplified soil-structure interaction analysis, is also indicated (dashed line).

justified, since the local heterogeneities on figure 1 are characterized by a much smaller length scale. Deeper soil layers will play a role in the dynamic soil-structure interaction in the frequency range around 10 Hz.

3. Telescope pier design

The T250 telescope is mounted on a concrete pier with a height of 15.25 m, founded on 73 reinforced concrete micro-piles with a diameter of 0.40 m (figures 5 and 6). The upper part of the pier is a truncated cone with an outer radius of 1.4 m at the top and 3.5 m at the base. The lower part of the telescope pier consists of a concrete cylinder with an outer radius of 3.5 m, reinforced with 7 radial ribs. The overall thickness of the pier is 0.6 m.

The telescope pier is supported by a ring shaped pile cap with an external radius of 5 m and an internal radius of 1.2 m. The pile cap has a height of 1.5 m. The opening in the pile cap acts as an elevator pit for the telescope lens lift.

The pier and the pile cap is constructed with HA-35 concrete with a Young's modulus $E = 35\,\mathrm{GPa}$, a Poisson's ratio $\nu = 0.2$ and a density $\rho = 2500\,\mathrm{kg/m^3}$. For the micro-piles, a high strength HA-45 concrete is used, with a Young's modulus $E = 37.5\,\mathrm{GPa}$, a Poisson's ratio $\nu = 0.2$ and a density $\rho = 2500\,\mathrm{kg/m^3}$. A material damping ratio $\beta_\mathrm{c} = 0.02$ is assumed for the concrete.

4. Coupled FE-BE model of the telescope pier

In order to study the effect of dynamic soil-structure interaction on the first resonance frequency of the telescope pier, a coupled FE-BE model is constructed. The telescope pier, the pile cap and the pile foundation are modelled with finite elements, whereas a boundary element model accounts for the infinite extent of the layered soil. In order to facilitate the BE modelling, a cylindrical soil volume with a radius of 5 m and a depth of 7.5 m is included in the FE model. In this way, the BE mesh is limited to the surface

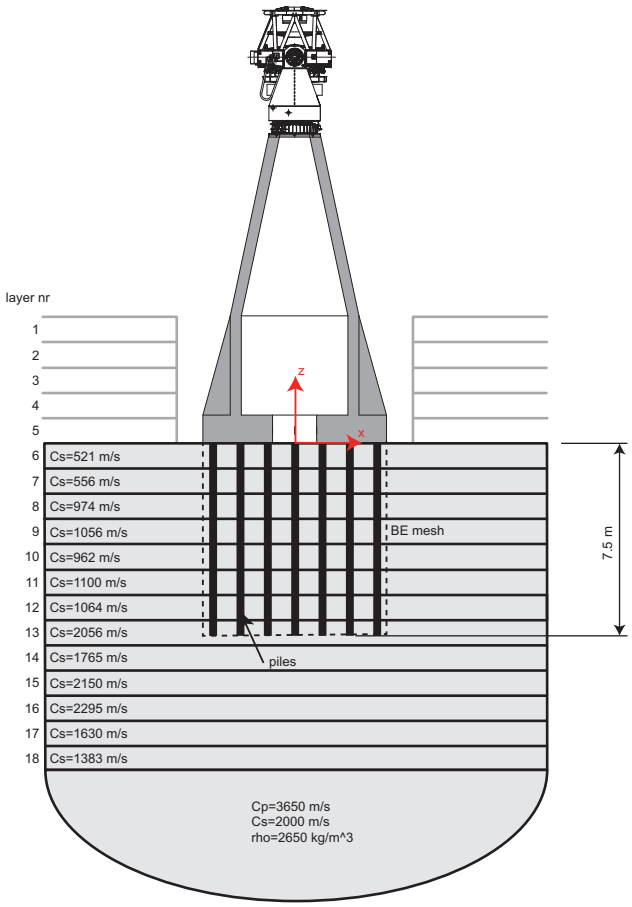

Figure 3: Coupled FE-BE model.

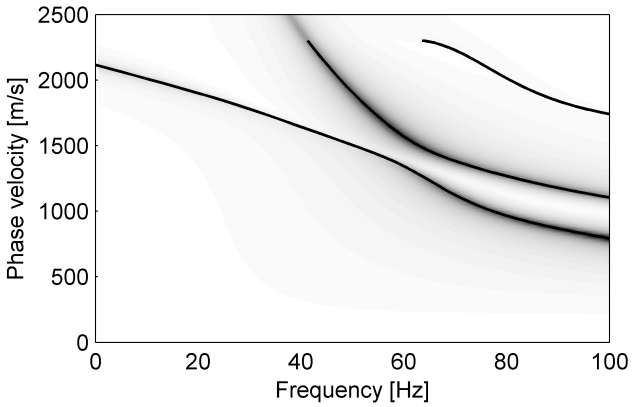

Figure 4: Spectrum of the vertical velocity $\tilde{v}_z(C_r, \omega)$ at the surface due to a vertical harmonic point load applied at the surface. The dispersion curves of the first three surface waves are also indicated (black lines).

of the soil cylinder (figure 3) and the surface of the 73 piles does not have to be included in the boundary element mesh.

The finite element (FE) model of the telescope pier, the pile cap, the micro-piles and the cylindrical soil volume is shown in figure 7. The origin of the right-handed Cartesian frame of reference (x, y, z) is located

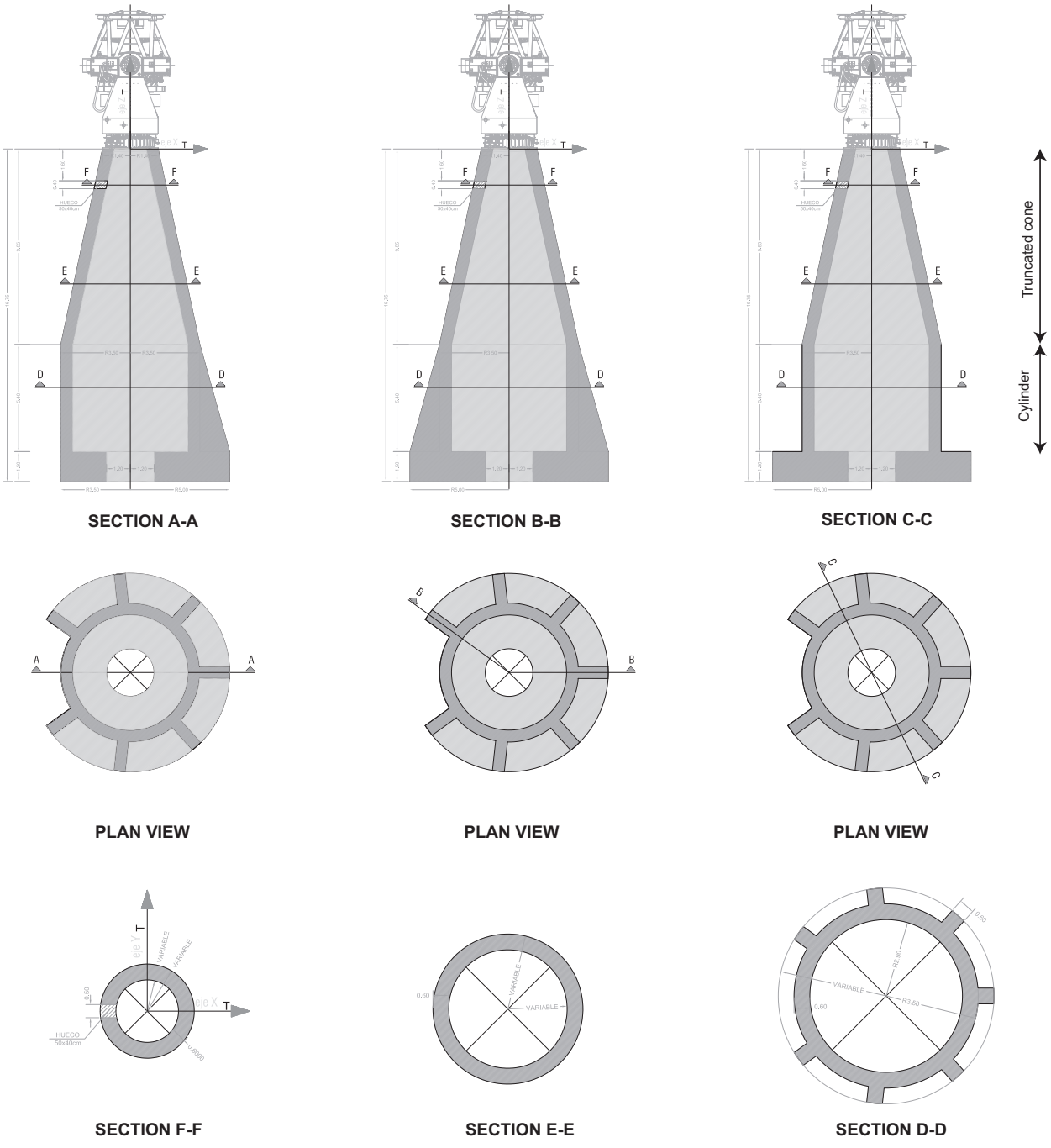

Figure 5: Elevation and cross section of the T250 telescope [9].

at ground level, with the x-axis along the center line of the notch in the pile cap and the z-axis pointing upwards (figures 3 and 7).

The telescope pier is meshed in Ansys with 1206 8-node rectangular Mindlin-Reissner shell elements with a thickness of 0.6 m. The pile cap and the cylindrical soil region are modelled with 1720 and 3200 20-node (quadratic) solid elements, respectively. The micro-piles are modelled with 584 beam elements, connected to the solid elements for the cylindrical soil region. The maximum element size equals 1 m.

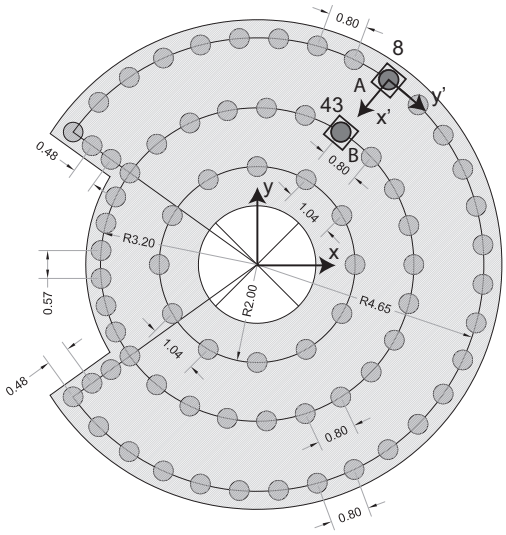

Figure 6: Layout of the pile foundation [9].

The telescope is represented by a rigid mass of 45000 kg, located at a distance of 3.15 m above the top of the pier. This is modelled as a concentrated mass in an auxiliary node ($x = 0$, $y = 0$, $z = 19.9\,\mathrm{m}$) with 6 degrees of freedom. Constraint equations are employed to couple the six rigid body modes of the top ring of the pier to the respective degrees of freedom of the concentrated mass.

The FE model (telescope pier, pile cap, pile foundation, and soil) is generated in Ansys and has 25898 nodes, 6711 elements, and 90888 degrees of freedom. The FE model is subsequently imported in Matlab, where the stiffness and mass matrices are assembled using the Matlab toolbox StaBIL [22].

A BE mesh is constructed that conforms with the finite elements on the surface of the cylindrical soil volume (figure 8). 8-node serendipity boundary elements are used with 6×6 Gaussian integration points per boundary element.

The BE system matrices are computed with the Matlab toolbox BEMFUN [23]. These BE system matrices relate the displacement and traction vectors at the BE nodes. At the edge of the bottom and side of the cylindrical soil volume, double nodes (one attached to the side surface and one to the bottom surface) are used to solve the BE corner problem (figure 8).

When a boundary element formulation is applied to dynamic soil-structure interaction problems with embedded foundations, inaccurate results may be obtained at frequencies that correspond to the eigenfrequencies of the finite domain that has been excavated. These frequencies are therefore referred to as fictitious eigenfrequencies [24, 25]. For the problem at hand, the soil is relatively stiff and the frequency content is relatively low; fictitious eigenfrequencies are therefore not expected. This is confirmed by a validation example in section 5. Techniques to mitigate fictitious eigenfrequencies, such as the Combined Helmholtz Integral Equation Formulation (CHIEF method) [26], are therefore not applied in the present analysis.

5. Model verification and validation

The correctness of the BE model is first verified with an analysis that only considers the soil in the coupled FE-BE model. A reference solution for wave propagation in the layered elastic halfspace, referred to as Green's functions, is obtained by means of the direct stiffness method [19, 20, 27] as implemented in the ElastoDynamics Toolbox (EDT) for Matlab [19].

The coupled FE-BE model is used to compute the response of the layered halfspace due to a unit harmonic load at point A ($x = 2.69\,\mathrm{m}$, $y = 3.80\,\mathrm{m}$, $z = 0\,\mathrm{m}$) along the z-direction. The location of point A corresponds to the head of micro-pile 8 (figure 6) for which the pile impedance has been measured in situ [28]. The micro-piles are not included in the present analysis, however.

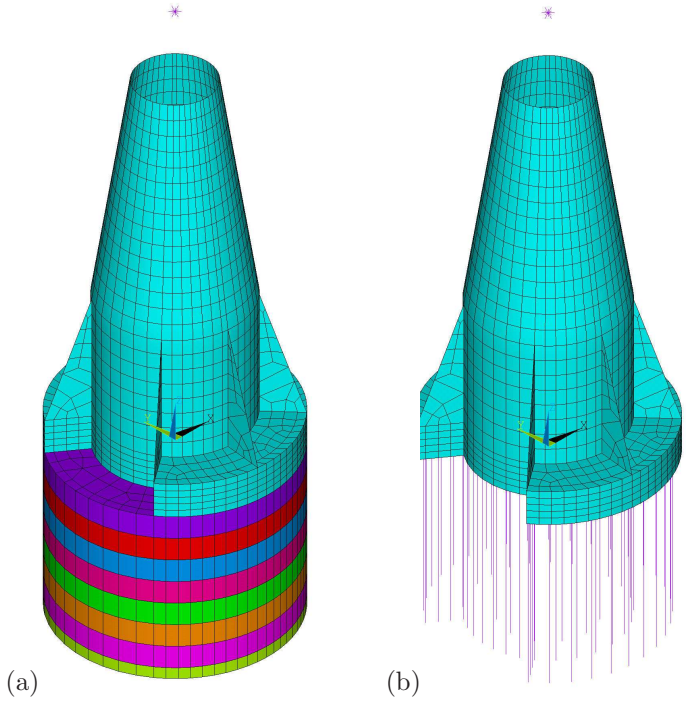

Figure 7: FE mesh of (a) the telescope pier, the pile cap, the soil and the micro-piles, and (b) the telescope pier, the pile cap, and the micro-piles. Different materials are indicated with different colors.

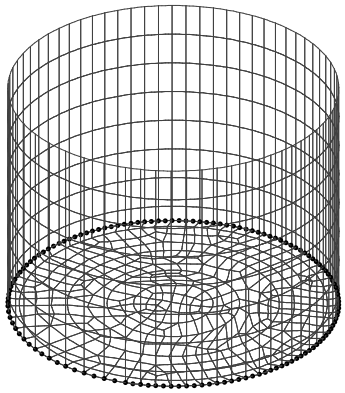

Figure 8: BE mesh of the cylindrical soil volume surrounding the micro-piles. The double corner nodes are indicated with black dots.

The response at point B ($x = 1.71\,\mathrm{m}$, $y = 2.70\,\mathrm{m}$, $z = 0\,\mathrm{m}$) is computed with the coupled FE-BE model. The location of point B corresponds to the head of micro-pile 43 (figure 6), for which the pile impedance has been measured in situ [28].

Figure 9 compares the receptance at point B due to unit harmonic loading in point A in the z-direction. Due to the relatively small distance between points A and B, the singular behavior of the fundamental solution dominates the response. This singular behavior is not accurately approximated by the finite element mesh, however, which results in a discrepancy between the results in figure 9. This difference can be reduced by a (local) mesh refinement around point A. Since the singular behavior is not present in further calculations,

no mesh refinement is performed, however.

Figure 10 compares the receptance at a point C ($x = -0.54\,\mathrm{m}$, $y = -4.97\,\mathrm{m}$, $z = 0\,\mathrm{m}$), further away from point A. Perfect correspondance is obtained, since the solution is not influenced by the singular behavior of the fundamental solution near the source point. Furthermore, the results of the coupled FE-BE model are free of fictitious eigenfrequencies in the frequency range under consideration.

Figure 11 compares the wave field on the surface of the layered halfspace due to vertical harmonic loading in point A in the z-direction to the reference solution. At all frequencies, the coupled FE-BE model is able to reproduce the cylindrical (Rayleigh) wave fronts and the correspondance between both solutions is perfect, as expected.

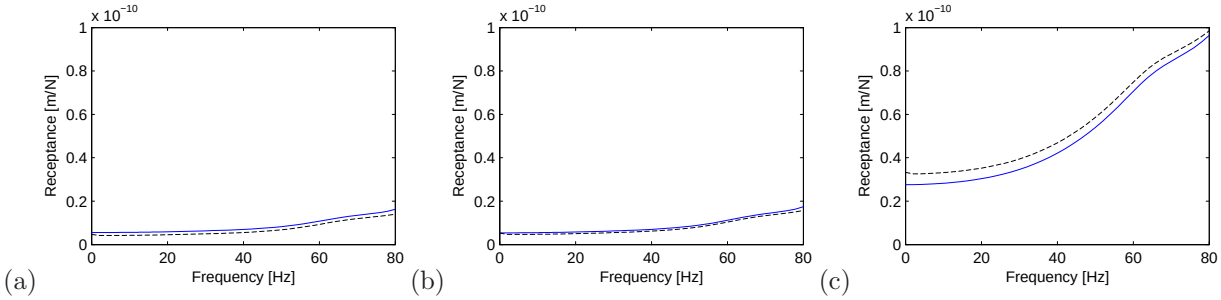

Figure 9: Receptance (a) u_x, (b) u_y, and (c) u_z at point B due to unit harmonic loading in point A in the z-direction. The solution of the coupled FE-BE model (solid line) is compared to the reference solution computed with the direct stiffness method (dashed line).

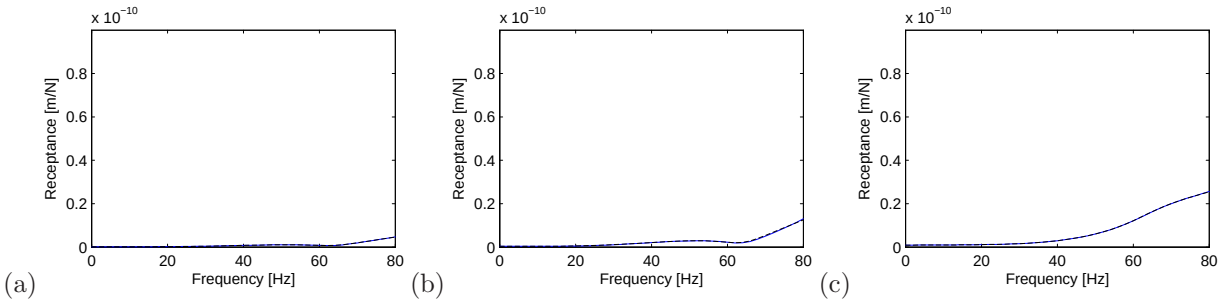

Figure 10: Receptance (a) u_x, (b) u_y, and (c) u_z at point C due to unit harmonic loading in point A in the z-direction. The solution of the coupled FE-BE model (solid line) is compared to the reference solution computed with the direct stiffness method (dashed line).

In order to validate the coupled FE-BE model, use is made of in situ measurements of the dynamic stiffness of piles A and B as indicated on figure 6 [28]. A cubic concrete pile head with a side of 0.5 m has been casted on top of piles A and B to facilitate sensor mounting using aluminium plates (figure 12). Since the orientation of the concrete blocks differs from the global coordinate system, a local coordinate system (x',y',z') has been defined, where the x'-axis is a radial axis pointing through the center of the foundation (figure 6). The angle between the x- and x'-axes equals 207.37°. Pile head A is located at ($x' = 0\,\mathrm{m}$, $y' = 0\,\mathrm{m}$, $z' = 0\,\mathrm{m}$) and pile head B at ($x' = 1.43\,\mathrm{m}$, $y' = -0.17\,\mathrm{m}$, $z' = 0\,\mathrm{m}$).

A total number of 100 impacts have been applied in the three positive directions (x',y',z') on pile A by means of an instrumented PCB 086D50 impact hammer with a mass of 9.79 kg. The response of the source pile has been measured in the three directions by means of charge accelerometers (figure 12). In addition, the response of the adjacent pile B has been measured with high-sensitivity accelerometers.

The transfer functions between the impact force and the pile head displacements have been determined from the 100 impacts. First, the mobility of pile heads A and B is considered for loading on pile head A in the x'-direction (figure 13). The 95% confidence bounds have been computed, assuming that the estimated

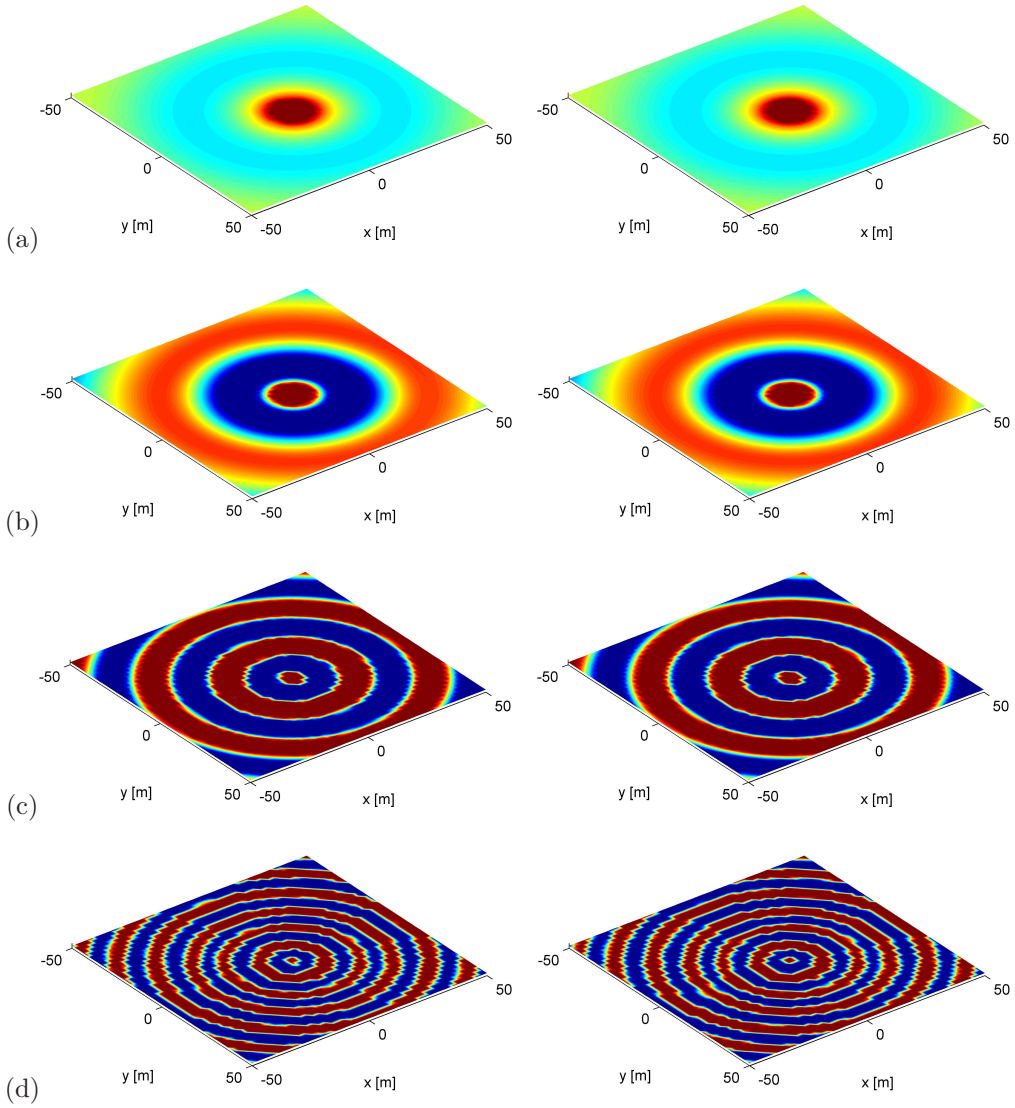

Figure 11: Real part of the vertical soil displacement at (a) 20 Hz, (b) 40 Hz, (c) 60 Hz, and (d) 80 Hz due to unit harmonic loading in point A in the z direction. The results obtained with the coupled FE-BE model (left) are compared to the results obtained with the direct stiffness method (right).

transfer function follows a Gaussian probability distribution, so that its modulus follows a Rice distribution. The bounds of the 95% confidence region of the modulus are computed as the inverse cumulative Rice distribution evaluated at 0.025 and 0.975.

At limiting high frequencies, the response of the loaded pile head A is expected to be governed by one-dimensional shear wave propagation in the pile. The mobility in the loading direction of the loaded pile (figure 13) should therefore converge to a value $1/Z = 1.3 \times 10^{-6}\,\mathrm{m/s/N}$ where $Z = \rho C_\mathrm{s} A$ is the impedance of the concrete pile with density $\rho = 2500\,\mathrm{kg/m^3}$, shear wave velocity $C_\mathrm{s} = 2500\,\mathrm{m/s}$, and cross section $A = 0.123\,\mathrm{m^2}$. In the other directions, the mobility is expected to vanish at limiting high frequencies. At the maximum frequency of 300 Hz (figure 13), the corresponding shear wavelength in the pile is equal to $\lambda_\mathrm{s} = 8.3\,\mathrm{m}$, which is larger than the pile length. Therefore, the limit value of the mobility of $1.3\times10^{-6}\,\mathrm{m/s/N}$ has not yet been reached and a higher value of $5.2 \times 10^{-6}\,\mathrm{m/s/N}$ is observed, as a result of the dynamic

Figure 12: Accelerometer configuration on the source and receiver piles.

interaction between the pile and the (softer) surrounding soil layers.

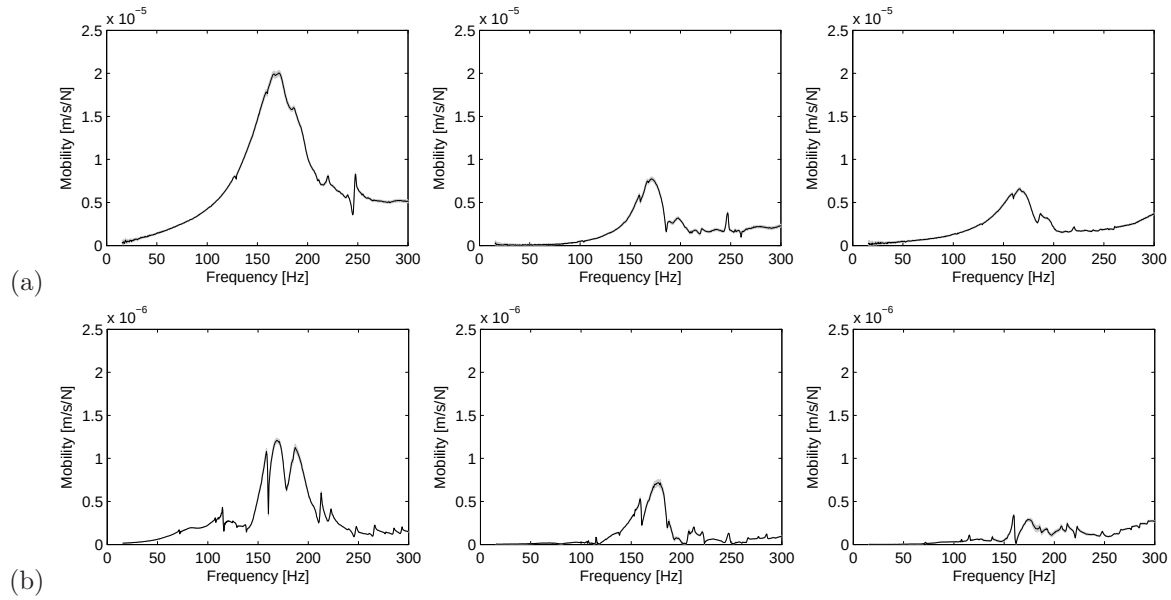

Figure 13: Mobility of pile heads (a) A and (b) B in the x'-direction (left), y'-direction (center), and z'-direction (right) for loading on pile head A in the x'-direction. The confidence bounds on the experimental results are indicated with a shaded area.

At frequencies below 15 Hz, a low coherence is observed in the measurements. This is a general shortcoming of impedance tests with an impact hammer at the soil's surface, as only the shallow soil layers are excited. At these low frequencies, the response is governed by the response of deeper soil layers (as indicated in section 2) that are difficult to excite by means of an impact hammer. For these reasons, the measured results below 15 Hz have been omitted. Alternatively, the use of a passive test using ambient vibration data [29] would have allowed to better measure the transfer function at low frequencies. In the following, the foundation impedance is validated in the frequency range from 15 to 80 Hz, since dynamic soil-structure interaction between (single) micro-piles and the soil is more apparent in this frequency range. At lower frequencies, the response is dominated by the (deeper) soil layers (as determined in the down hole test) and the response of the pile group as a whole, which is studied in the following section.

The pile impedance tests are simulated with the coupled FE-BE model, that includes the micro-piles embedded in the soil, without the pile cap and conical support structure. This allows to compare the

mobility at pile heads A and B with the experimental results (figures 14 to 16) for impact on pile A in the three directions.

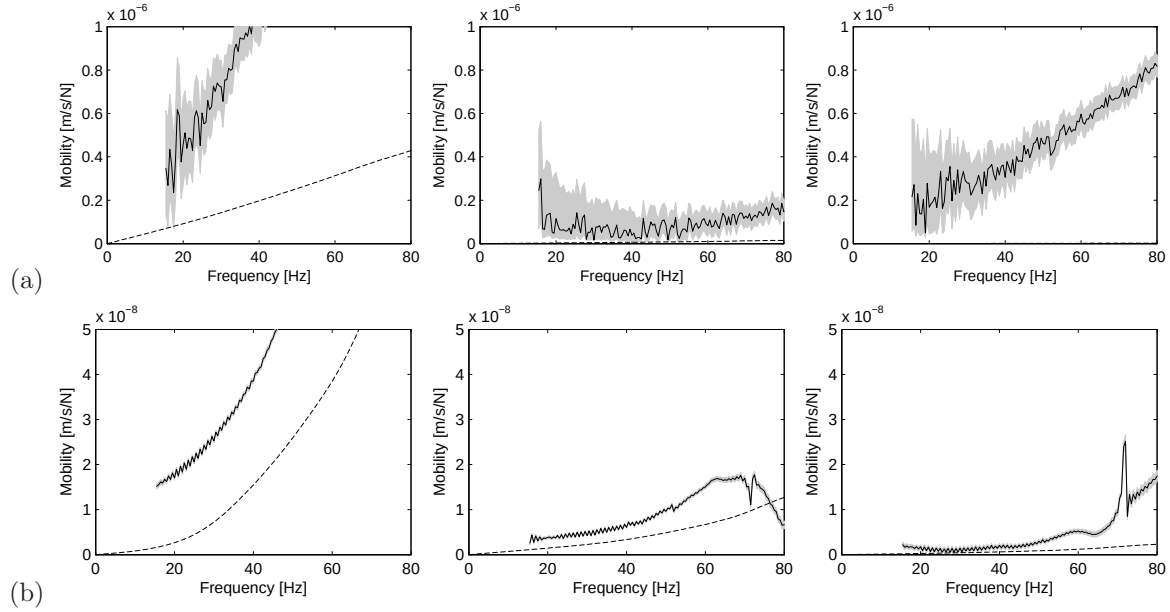

Figure 14: Mobility of pile heads (a) A and (b) B in the x'-direction (left), y'-direction (center), and z'-direction (right) for loading on pile head A in the x'-direction. The numerical results (dashed lines) are compared to the experimental values (solid lines). The confidence bounds on the experimental results are indicated with a shaded area.

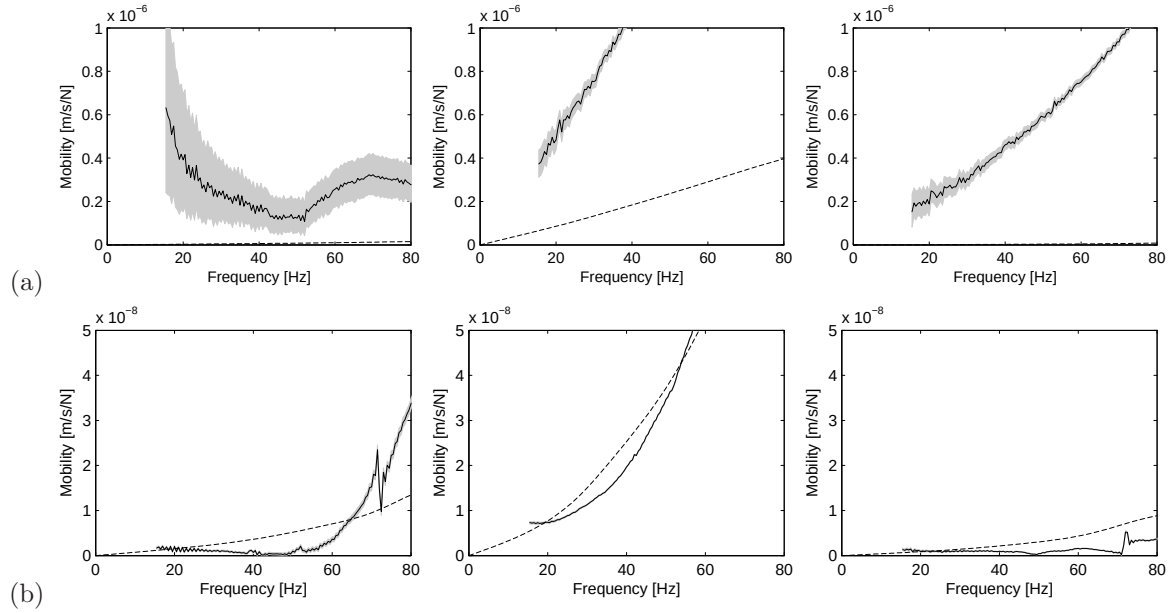

Figure 15: Mobility of pile heads (a) A and (b) B in the x'-direction (left), y'-direction (center), and z'-direction (right) for loading on pile head A in the y'-direction. The numerical results (dashed lines) are compared to the experimental values (solid lines). The confidence bounds on the experimental results are indicated with a shaded area.

The numerical results obtained in the frame of reference (x,y,z) are transformed to the frame of reference

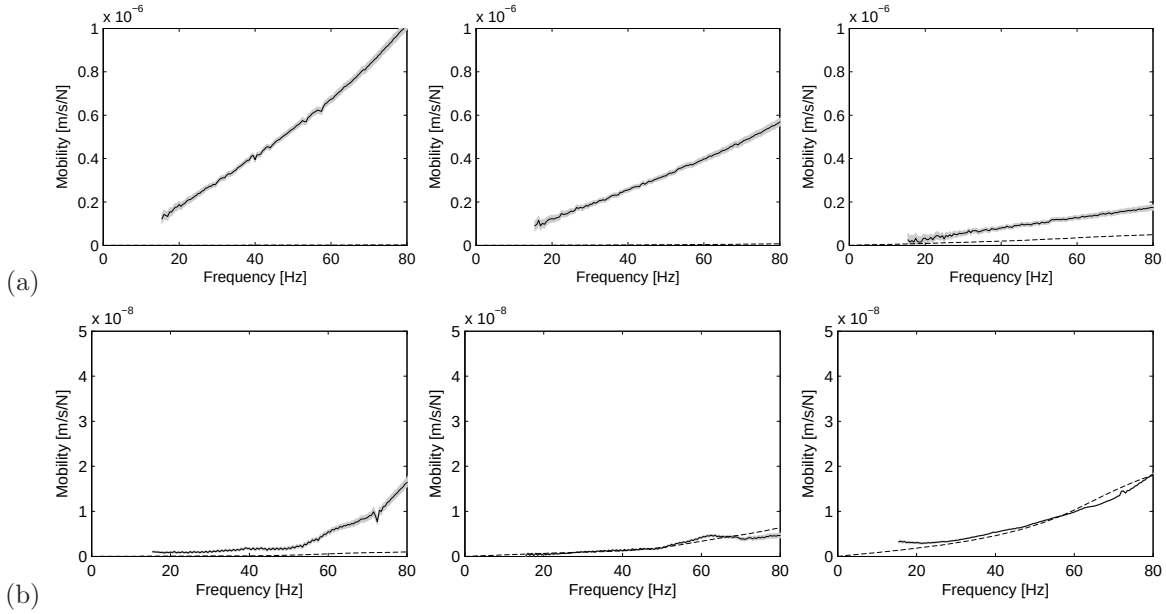

Figure 16: Mobility of pile head (a) A and (b) B in the x'-direction (left), y'-direction (center), and z'-direction (right) for loading on pile head A in the z'-direction. The numerical results (dashed lines) are compared to the experimental values (solid lines). The confidence bounds on the experimental results are indicated with a shaded area.

(x', y',z') used in the experimental setup.

First, the response due to horizontal loading in the x'-direction is considered (figure 14). The response of source pile A in the loading direction x' is underestimated by a factor of about 4. For the response in the directions y' and z', the discrepancy is even more pronounced. The numerical model predicts a very small response of source pile A in the y'- and z'-directions due to the large axial stiffness of the pile, while the measured mobility is of the same order of magnitude as in the x'-direction. The discrepancy is attributed to the sensor placement on the loaded pile. As can be seen on figure 12, the sensors have been placed on the edges of the pile head. Similarly, the impacts have been applied off-centered. For the horizontal loading under consideration, the numerical model predicts no significant vertical response of the pile head as a result of the large axial stiffness of the pile. Since the accelerometer is placed eccentrically on the pile head, however, the rotation of the pile head results in a vertical response. Off-centered impacts during the in situ tests have a similar influence on the measured response. Furthermore, the response in the y'-direction, perpendicular to the loading direction x' should be small from a theoretical point of view. In the case of horizontal loading in figure 14, an off-centered impact on the pile head results in a torsional reponse of the pile head that is not included in the numerical model but may give rise to a significant response in the y'-direction. The response of the receiver pile B show a similar difference.

A similar conclusion can be drawn for horizontal loading of pile head A in the y'-direction (figure 15). The response of source pile A in the loading direction y' is underestimated by a factor of about 4. For the response in the other directions x' and z', the discrepancy is even larger. The discrepancy is attributed to the fact that the sensors have been placed on the edges of the pile head and that impacts have been applied off-centered. For the horizontal loading, the numerical model predicts no significant vertical response of the pile head as a result of the large axial stiffness of the pile. Off-centered placement of accelerometers and off-centered impacts result in the rotation of the pile head and a corresponding large vertical response. The response of the receiver pile B in the y'-direction is well predicted, whereas a discrepancy is observed in the other directions.

For vertical loading on pile head A (figure 16), both the predicted and measured vertical response of pile head A are small due to the large axial stiffness of the pile. However, the response of source pile A

in the loading direction z' is underestimated. This may be attributed to the off-centered placement of accelerometers and off-centered impacts. An overestimation of the dynamic soil stiffness of the deeper soil layer could also explain the discrepancy between the experimental results and the numerical predictions, though this hypothesis is not supported by the geotechnical study. For the response in the horizontal directions x' and y', the discrepancy is very large and attributed to the sensor placement on the pile heads. The response of pile head B is well predicted in the y'- and z'-directions, whereas a larger difference is observed in the x'-direction.

Despite the inherent difficulty in predicting the in situ pile impedance, it is expected that the model is well suited to predict the response at lower frequencies, where dynamic soil-structure interaction is dominated by the (deeper) soil layers and the response of the pile group as a whole.

6. The effect of dynamic soil-structure interaction on the pier response

6.1. Analysis without dynamic soil-structure interaction

In a first analysis, the natural frequencies of the telescope structure are computed disregarding the effects of dynamic soil-structure interaction. This first estimate of the natural frequencies can be checked against the minimal required value of 10 Hz.

The FE model of the telescope, its supporting conical structure and the pile cap is considered. The pile cap is fixed at its base and the pile foundation is disregarded. The eigenmodes and eigenfrequencies of this structure clamped at its base are computed, as well as the dynamic response of the structure when subjected to unit harmonic horizontal loading.

Figure 17 shows the first 4 mode shapes, identified as bending modes of the telescope pier. The first eigenfrequency of the structure equals 14.3 Hz, which is well above the limit of 10 Hz imposed by the telescope manufacturer.

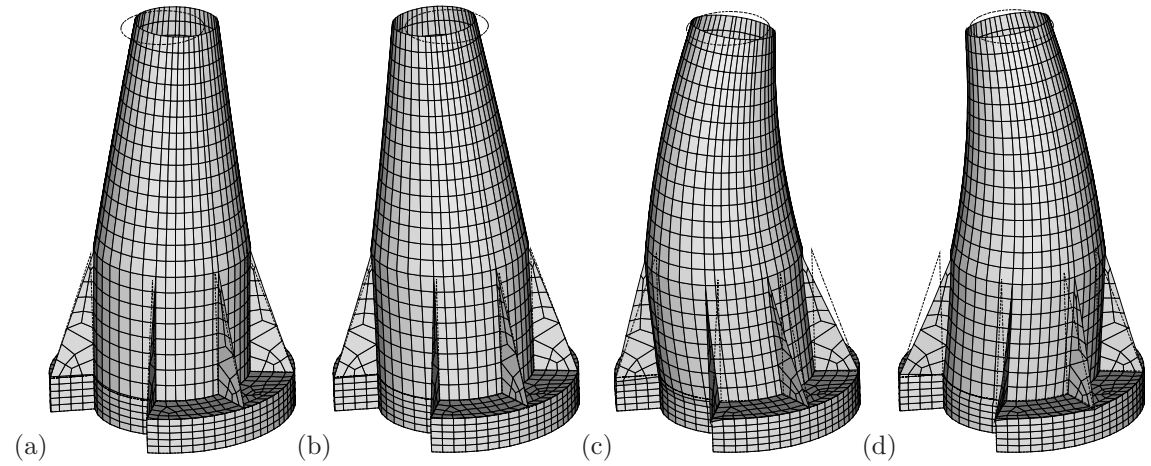

Figure 17: Eigenmodes of the structure fixed at its base: (a) mode 1 at 14.3 Hz, (b) mode 2 at 15.1 Hz, (c) mode 3 at 41.7 Hz, and (d) mode 4 at 42.4 Hz.

Next, a unit harmonic point load in the x-direction is applied at the concentrated mass of 45000 kg that represents the telescope. Figure 18 shows the displacement of the concentrated mass in the direction of the loading, dominated by the first structural mode at 14.28 Hz. The width of the resonance peak allows to estimate the modal damping using the half-power bandwidth method [30] as $\xi = 0.021$. This modal damping is entirely attributed to the assumed material damping in the concrete.

6.2. Dynamic soil-structure interaction analysis

In order to study the effect of dynamic soil-structure interaction on the resonance frequency, the response of the telescope pier due to a unit harmonic point load in the x-direction applied at the concentrated mass

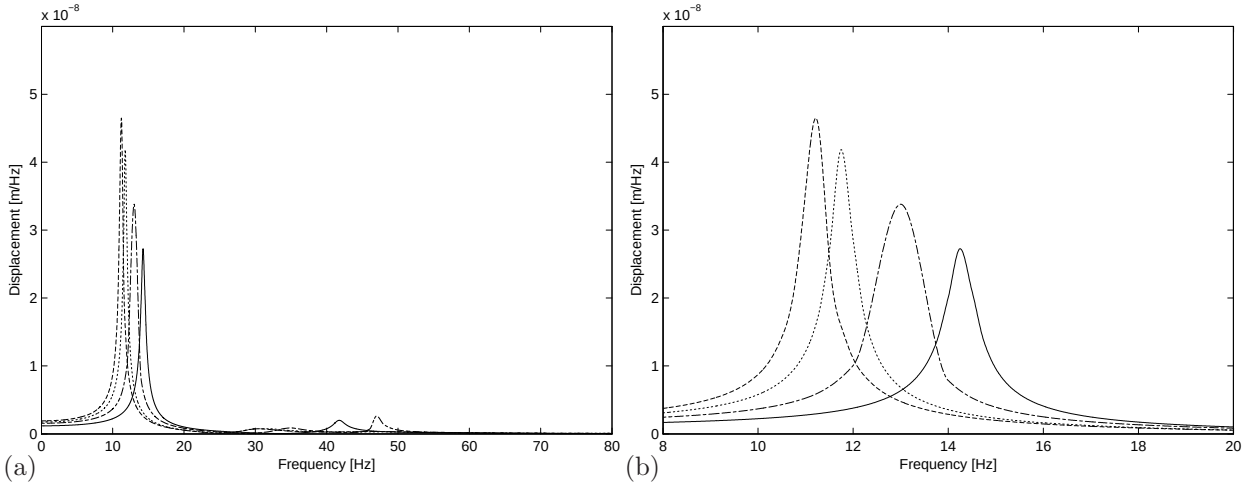

Figure 18: (a) Modulus of the displacement of the top of the telescope due to a unit harmonic horizontal load applied at the concentrated mass, and (b) zoom around the resonance peak. Results are plotted for an analysis without dynamic soil-structure interaction (solid black line), with dynamic soil-structure interaction (dashed line), with dynamic soil-structure interaction and a rigid pile cap (dotted line), and with a simplified approach (dash-dotted line).

of 45000 kg is computed. The complete FE-BE model is considered, which includes the telescope pier, the pile cap, the pile foundation and the cylindrical soil region.

Figure 18 shows the displacement of the concentrated mass in the direction of the loading. The response of the telescope, loaded by a harmonic point load at the top, is dominated by a resonance peak corresponding to the first bending mode of the telescope pier. The peak response occurs at 11.2 Hz, which is significantly lower than the resonance frequency at 14.3 Hz in the reference analysis for the structure fixed at its base. This demonstrates the importance of dynamic interaction between the pile foundation and the soil. The resonance peak has a larger amplitude than the resonance peak of the telescope pier fixed at its base. The resonance frequency at 11.2 Hz is higher than the limit imposed by the telescope manufacturer to avoid malfunctioning of the equipment, which confirms that the imposed design criteria are met.

The modal damping ratio is estimated using the half-power bandwidth method as $\xi = 0.021$, which is very similar as the value obtained without accounting for dynamic soil-structure interaction. This demonstrates that radiation damping in the soil does not importantly contribute to the damping ratio associated with the fundamental mode. This can be explained by the fact that, at the resonance peak, the dimensionless frequency $a_0 = \omega R/C_{\mathrm{s}}^{\mathrm{ref}} = 0.07$ is relatively low, with R the radius of the embedded cylindrical foundation and $C_{\mathrm{s}}^{\mathrm{ref}} = 890\,\mathrm{m/s}$ the reference shear wave velocity of the soil.

The corresponding radiated wave field in the soil at 20, 40, 60 and 80 Hz, is shown in figure 19. At 20 Hz, the wavelength in the soil is much larger than the dimensions of the telescope, substantiating that deeper soil layers will play an important role at the resonance frequency of the telescope. At higher frequencies, the wavelength and corresponding penetration depth of Rayleigh surface waves is smaller. At these frequencies, the deeper soil layers are of less importance and the dynamic interaction between the pier and the soil is determined by the top soil layers.

6.3. Dynamic soil-structure interaction analysis with a rigid pile cap

The coupled FE-BE model is computationally expensive, which is due to the evaluation of dynamic soil-structure interaction. During the design process, however, a fast computation is desirable. Therefore, it is investigated to what extent the FE-BE model can be simplified in order to reduce computation time.

A first simplification consists of neglecting the flexibility of the pile cap. While this assumption may result in an artificial increase of the stiffness of the supporting structure, the assumption of a rigid pile cap allows the use of impedance functions [31–33] in a dynamic soil-structure interaction analysis. The frequency

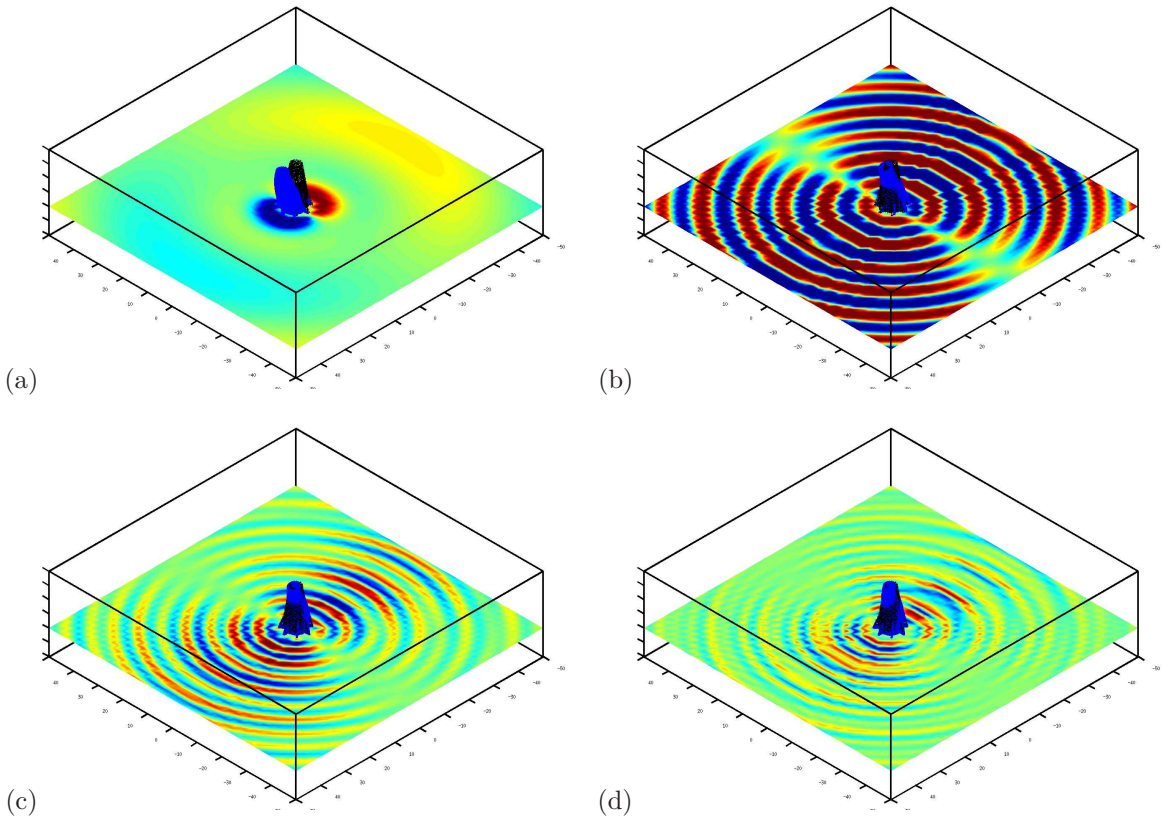

Figure 19: Real part of the vertical soil displacement at (a) 20 Hz, (b) 40 Hz, (c) 60 Hz, and (d) 80 Hz due to a horizontal harmonic load at the top of the telescope.

dependent elements $S_{mn}(a_0)$ of the 6×6 impedance matrix of a rigid foundation are commonly written in the following dimensionless form [33]:

$$S_{mn}(a_0) \quad = \quad K^{\mathrm{s}}_{mn} \left[K_{mn}(a_0) + i C_{mn}(a_0) \right] \tag{1}$$

where the subscripts m and n denote the horizontal (h), vertical (v), rotational (r) and torsional (t) degrees of freedom, while the static stiffness coefficients K^{s}_{mn} are defined as $K^{\mathrm{s}}_{\mathrm{hh}} = K^{\mathrm{s}}_{\mathrm{vv}} = \mu R$, $K^{\mathrm{s}}_{\mathrm{rr}} = K^{\mathrm{s}}_{\mathrm{tt}} = \mu R^3$ and $K^{\mathrm{s}}_{\mathrm{hr}} = \mu R^2$, with $\mu = \rho {C^{\mathrm{ref}}_{\mathrm{s}}}^2$ the (reference) shear modulus of the soil. The dimensionless stiffness and damping coefficients $K_{mn}(a_0)$ and $C_{mn}(a_0)$ depend on the dimensionless frequency $a_0 = \omega R / C^{\mathrm{ref}}_{\mathrm{s}}$ where R is the radius of the embedded cylindrical foundation.

In the literature, the imaginary part of the dynamic stiffness matrix is commonly divided by a_0. This is interesting in simple cases where the imaginary part remains more or less linear, such as for rigid surface foundations. In the case of a pile group, this is not relevant; therefore, this practice is not followed here.

Figure 20 shows the dimensionless stiffness and damping coefficients for the pile foundation with a rigid massless pile cap, where an average shear wave velocity $C^{\mathrm{ref}}_{\mathrm{s}} = C^{\mathrm{av}}_{\mathrm{s}} = 815.65\,\mathrm{m/s}$ and a density $\rho = 2400\,\mathrm{kg/m^3}$ are considered to compute the dimensionless foundation characteristics.

The horizontal stiffness coefficient is small with respect to the vertical stiffness, which is in correspondance with the large vertical stiffness of the single piles as observed in section 5. As a result, the vertical response of the telescope structure is less influenced by dynamic soil-structure interaction. Furthermore, the coupling between the rotational and torsional degrees of freedom is negligibly small. For the large pile group under consideration, it is expected that the impedance curves show large variations at higher frequencies ($a_0 >> 1$).

The dynamic soil stiffness of the massless, rigid pile cap is added to the FE model using constraint

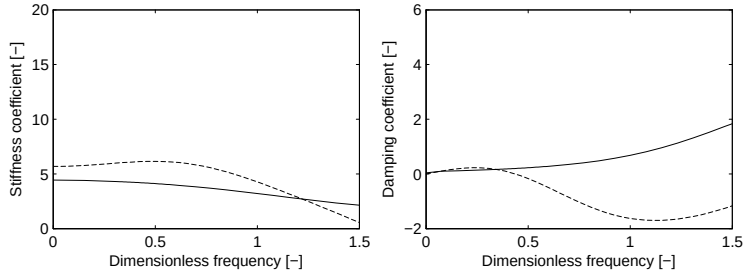

(a) k_{hh} c_{hh}

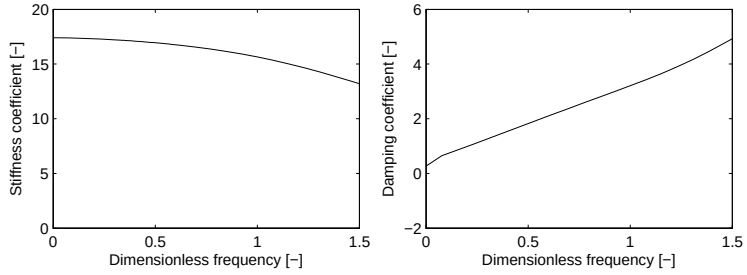

(b) k_{vv} c_{vv}

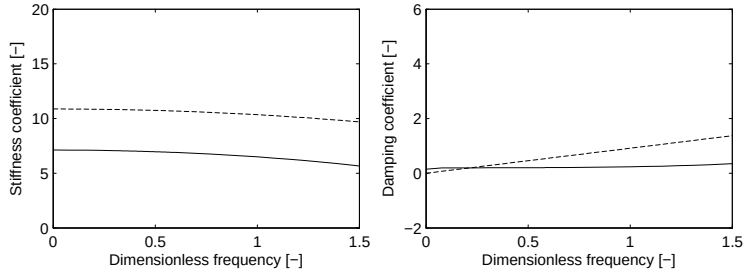

(c) k_{rr} c_{rr}

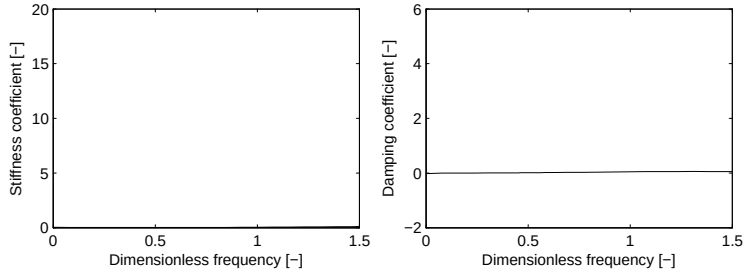

(d) k_{rh} c_{rh}

Figure 20: Stiffness (left) and damping (right) coefficients of the pile group with a rigid massless cap for the (a) horizontal, (b) vertical, (c) rocking and (d) horizontal-rocking rigid body modes. The results obtained with the coupled FE-BE model (solid line) are compared with results obtained with a simplified model by Taherzadeh et al. [17] (dashed line) for the horizontal and rocking motion.

equations, imposing a rigid body displacement to the base of the pile cap. Figure 18 shows the displacement of the concentrated mass in the direction of the loading. The resonance peak related to the first bending mode occurs at a frequency of 11.7 Hz. The increase of the frequency with respect to the model with a flexible pile cap (11.2 Hz) is due to the assumption of a rigid pile cap, resulting in a higher dynamic soil stiffness. It can hence be concluded that the flexibility of the pile cap has a minor effect on the resonance frequency of the telescope pier.

The assumption of a rigid pile cap still requires a computationally expensive coupled FE-BE analysis. Therefore, it is further investigated to what extent the model can be simplified through the use of approximate foundation impedance functions for pile groups.

A first simplified approach is to use Winkler springs for the soil, neglecting the effect of radiation damping and inertial effects [34]. Alternatively, the soil-pile system can be replaced by a single degree of freedom system [11, 35]. An overview of such simplified methodologies is given by Maravas et al. [36]. Since such an approach cannot account for the interaction between piles in a pile group, Dobry and Gazetas [32] have proposed a formulation that accounts for the dynamic interaction between the piles by modelling two-dimensional wave propagation between piles in the group. This model has been further refined to account for multiple wave reflections in the pile group [37, 38]. However, only a few attempts have been made to apply this technique to large groups of end-bearing piles, since the complex interaction between the piles results in a strong frequency dependence of the dynamic soil stiffness [39, 40].

An alternative approach developed by Taherzadeh et al. [17] is applied here for the calculation of the horizontal and rocking components K_{hh} and K_{rr} of the dynamic stiffness matrix, which dominate the response of the pile cap. The simplified model is composed of masses, springs and dampers (figure 21) characterized by the following parametrization [17]:

$$\chi = \lambda_0 \left(\frac{R}{H}\right)^{\lambda_1} \left(\frac{L_0}{s}\right)^{\lambda_2} \left(\frac{\rho_{\mathrm{b}} C_{\mathrm{s}}^{\mathrm{b}}}{\rho_{\mathrm{l}} C_{\mathrm{s}}^{\mathrm{l}}}\right)^{\lambda_3} \tag{2}$$

where R is the pile cap radius, H is the thickness of the soil layer, $L_0 = (E_{\mathrm{p}} I_{\mathrm{p}}/E_l)^{0.25}$ (with $E_{\mathrm{p}} I_{\mathrm{p}}$ the pile bending stiffness and E_l the Young's modulus of the soil layer) is the critical pile length, and s is the pile separation. ρ_{b} and ρ_{l} are the density of the bedrock and the soil layer, respectively. Similarly, $C_{\mathrm{s}}^{\mathrm{b}}$ and $C_{\mathrm{s}}^{\mathrm{l}}$ are the shear wave velocities of the bedrock and the soil layer. The parameters λ_0 to λ_3 have been tuned for each of the components in the simplified model against the results of coupled FE-BE calculations for rectangular rigid pile caps founded on a group of evenly spaced piles.

The parametrization (2) reduces to the model of a floating pile group if the properties of the bedrock and the soil layer correspond ($\rho_{\mathrm{b}} = \rho_{\mathrm{l}}$ and $C_{\mathrm{s}}^{\mathrm{l}} = C_{\mathrm{s}}^{\mathrm{b}}$). The model accounts for the effect of friction along the pile through the factor $\left(\rho_{\mathrm{b}} C_{\mathrm{s}}^{\mathrm{b}} / \left(\rho_{\mathrm{l}} C_{\mathrm{s}}^{\mathrm{l}}\right)\right)^{\lambda_3}$, which is considered to significantly contribute to the overall vertical impedance for the pile group under consideration.

In order to apply the approximate model of Taherzadeh et al. [17], the multi-layered halfspace in figure 2 is simplified as a single layer of 7 m on a halfspace. The shear wave velocity $C_{\mathrm{s}}^{\mathrm{l}} = 815.65$ m/s and the dilatational wave velocity $C_{\mathrm{p}}^{\mathrm{l}} = 1936.7$ m/s of the layer are chosen so that the wave travel times are the same as in the top 7 m of the multi-layered halfspace. Furthermore, an average density $\rho_{\mathrm{l}} = 2364\ \mathrm{kg/m^3}$ is considered. Since the piles are unevenly distributed over the pile cap and the pile cap has a notch and an opening, an average value for the pile separation $s = 1\,\mathrm{m}$ is computed by evenly distributing 73 piles over an equivalent square foundation with a side $B = \sqrt{\pi R^2} = 8.9\,\mathrm{m}$.

Figure 20 compares the dynamic stiffness and damping coefficients obtained with both models. Both the horizontal and rocking components are strongly over-estimated by the simplified model. This will result in an overestimation of the first resonance peak. The damping coefficient for the horizontal mode is underestimated by the model, whereas the damping for the rocking deformation is overestimated.

Figure 18 shows the response of the telescope pier computed with the simplified pile cap model. Since the simplified pile cap model overestimates the dynamic stiffness of the pile group, the corresponding resonance peak is located at a higher frequency of about 13 Hz. As a result, the use of the simplified approach over-estimates the first resonance frequency for the present analysis.

The discrepancy is attributed to the fact that the foundation is not rectangular, that the pile spacing is not constant and that the top soil layers and the bedrock are not homogeneous. The extrapolation (2) results in a large error if the geometry and soil layering of the problem are different from the square pile caps with a constant pile separation for which the parameters have been tuned.

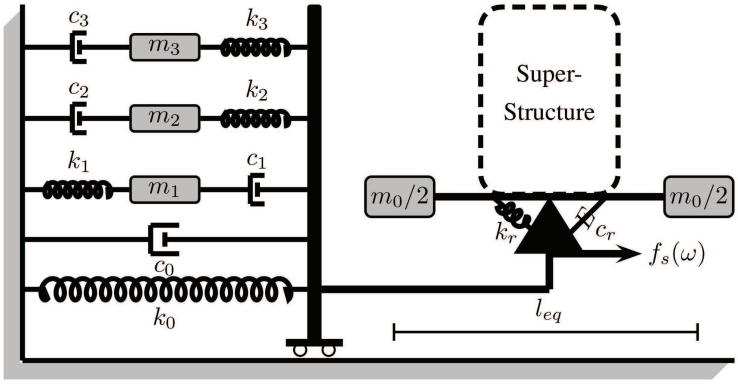

Figure 21: Lumped parameter model for the soil, consisting of a set of masses, springs and dampers [17].

7. Conclusion

In this paper, the dynamic soil-structure analysis of the telescope pier of the Observatorio Astrofísico de Javalambre (OAJ, Javalambre Astrophysical Observatory) has been performed. Since astrophysical observations may be hindered by mechanical vibration of optical equipment due to wind loading, the telescope manufacturer has imposed a minimal natural frequency of 10 Hz for the supporting structure. A first analysis that disregards dynamic soil-structure interaction has been performed, where the telescope pier is fixed at its base. The response of the telescope, loaded by a harmonic point load at the top, is dominated by the bending modes of the telescope pier. The first eigenfrequency of the telescope pier equals 14.3 Hz, which is well above the imposed limit of 10 Hz.

The results of a coupled FE-BE calculation have clearly demonstrated a significant effect of dynamic soil-structure interaction which causes the resonance peak to shift down to 11.2 Hz.

Furthermore, it has been investigated to what extent the FE-BE model can be simplified in order to reduce computation time. The assumption of a rigid pile cap allowed to account for dynamic soil-structure interaction in a simplified way, through the use of stiffness and damping coefficients. The resulting resonance frequency of 11.7 Hz computed with this approach demonstrates that the flexibility of the pile cap has a minor effect on the resonance frequency of the telescope pier.

The use of an analytical model for the pile group results in an overestimation of the dynamic soil stiffness. This error is due to the large difference between the actual geometry and the square pile cap model for which the parameters have been tuned.

Acknowledgements

The authors would like to thank Torrescamara for providing the geotechnical data as well as the geometrical and material properties of the telescope pier needed for the dynamic soil-structure interaction analysis. The first author is a postdoctoral fellow of the Research Foundation - Flanders (FWO). All financial support is hereby gratefully acknowledged.

References

[1] A. Cenarro, M. Moles, D. Cristóbal-Hornillos, N. Gruel, N. Benítez, A. Marín-Franch, The Javalambre Astrophysical Observatory project, in: SPIE Astronomical Telescopes and Instrumentation: Observational Frontiers of Astronomy for the New Decade, International Society for Optics and Photonics, 2010.

[2] A. Cenarro, M. Moles, D. Cristóbal-Hornillos, A. Marín-Franch, N. Gruel, A. Yanes-Díaz, S. Chueca, J. Varela, A. Ederoclite, F. Rueda-Teruel, The Observatorio Astrofisico de Javalambre: goals and current status, in: SPIE Astronomical Telescopes+ Instrumentation, International Society for Optics and Photonics, 2012.

[3] A. Cenarro, D. Cristóbal-Hornillos, N. Gruel, A. Marin-Franch, M. Moles, L. Valdivielso, K. Viironen, The Observatorio Astrofísico de Javalambre: telescopes and instrumentation, in: Highlights of Spanish Astrophysics VI, Proceedings of the IX Scientific Meeting of the Spanish Astronomical Society, 2010.

[4] S. Chueca, A. Marín-Franch, A. Cenarro, J. Varela, A. Ederoclite, D. Cristóbal-Hornillos, C. Hernández-Monteagudo, N. Gruel, M. Moles, A. Yanes, Curvature wavefront sensing performance simulations for active correction of the Javalambre wide-field telescopes, in: SPIE Astronomical Telescopes+ Instrumentation, International Society for Optics and Photonics, 2012.

[5] A. Guesalaga, B. Neichel, F. Rigaut, J. Osborn, D. Guzman, Comparison of vibration mitigation controllers for adaptive optics systems, Applied optics 51 (19) (2012) 4520–4535.

[6] M. Moles, S. Sánchez, J. Lamadrid, A. Cenarro, D. Cristóbal-Hornillos, N. Maicas, J. Aceituno, Site testing of the Sierra de Javalambre: First results, Publications of the Astronomical Society of the Pacific 122 (889) (2010) 363–372.

[7] M. Moles, A. Cenarro, D. Cristóbal-Hornillos, N. Gruel, A. M. Franch, L. Valdivielso, K. Viironen, The Observatorio Astrofísico de Javalambre. a planned facility for large scale surveys, in: Highlights of Spanish Astrophysics VI, Proceedings of the IX Scientific Meeting of the Spanish Astronomical Society, 2010.

[8] D. G. MacMynowski, G. Z. Angeli, K. Vogiatzis, J. Fitzsimmons, S. Padin, Parametric modeling and control of telescope wind-induced vibration, in: Astronomical Telescopes and Instrumentation, International Society for Optics and Photonics, 2004, pp. 266–277.

[9] Geodeser, Estudio geológico-geotécnico. Observatorio Astrofísico del Pico del Buitre, Tech. rep., Geodeser (2009).

[10] D. Beskos, T. Krauthammer, I. Vardoulakis (Eds.), Dynamic soil-structure interaction, A.A. Balkema, 1984.

[11] J. Wolf, Dynamic soil-structure interaction, Prentice-Hall, Englewood Cliffs, New Jersey, 1985.

[12] O. Von Estorff, C. Hagen, Iterative coupling of FEM and BEM in 3D transient elastodynamics, Engineering Analysis with Boundary Elements 29 (2005) 775–787.

[13] G. Pavlatos, D. Beskos, Dynamic elastoplastic analysis by BEM/FEM, Engineering Analysis with Boundary Elements 14 (1) (1994) 51–63.

[14] D. Soares, O. von Estorff, W. J. Mansur, Iterative coupling of BEM and FEM for nonlinear dynamic analyses, Computational Mechanics 34 (2004) 67–73.

[15] D. Clouteau, M. Elhabre, D. Aubry, Periodic BEM and FEM-BEM coupling: application to seismic behaviour of very long structures, Computational Mechanics 25 (2000) 567–577.

[16] D. Clouteau, R. Cottereau, G. Lombaert, Dynamics of structures coupled with elastic media. A review of numerical models and methods, Journal of Sound and Vibration 332 (2013) 2415–2436.
URL `http://dx.doi.org/10.1016/j.jsv.2012.10.011`

[17] R. Taherzadeh, D. Clouteau, R. Cottereau, Simple formulas for the dynamic stiffness of pile groups, Earthquake Engineering and Structural Dynamics 38 (15) (2009) 1665–1685.

[18] B. Consulting, Reconocimiento geofísico básico mediante sísmica de refracción, tomografía eléctrica, down-hole, cross-hole y sondeo eléctrico vertical (SEV). Observatorio Astroifísico del Pico del Buitre, Tech. rep., B.G.H. (2009).

[19] M. Schevenels, S. François, G. Degrande, EDT: An ElastoDynamics Toolbox for MATLAB, Computers & Geosciences 35 (8) (2009) 1752–1754.
URL `http://dx.doi.org/10.1016/j.cageo.2008.10.012`

[20] E. Kausel, J. Roësset, Stiffness matrices for layered soils, Bulletin of the Seismological Society of America 71 (6) (1981) 1743–1761.

[21] G. Rix, C. Lai, Simultaneous inversion of surface wave velocity and attenuation, in: Proceedings of the First International conference on Site Characterization, Rotterdam, 1998, pp. 503–508.

[22] D. Dooms, G. De Roeck, G. Degrande, S. François, Een interactieve en adaptieve toepassing voor de statische en dynamische analyse van structuren (StaBIL), Tech. Rep. BWM-2009-21, Department of Civil Engineering, KU Leuven (October 2009).

[23] S. François, M. Schevenels, G. Degrande, BEMFUN: MATLAB toolbox for boundary elements in elastodynamics. Version 2.1 Build 16, User's guide BWM-2009-26, Department of Civil Engineering, KU Leuven (December 2009).

[24] L. Pyl, D. Clouteau, G. Degrande, A weakly singular boundary integral equation in elastodynamics for heterogeneous domains mitigating fictitious eigenfrequencies, Engineering Analysis with Boundary Elements 28 (12) (2004) 1493–1513.
URL `http://dx.doi.org/10.1016/j.enganabound.2004.08.001`

[25] H. Schenck, Improved integral formulation for acoustic radiation problems, Journal of the Acoustical Society of America 44 (1968) 41–58.

[26] M. Bonnet, Boundary integral equation methods for solids and fluids, John Wiley and Sons, Chichester, United Kingdom, 1995.

[27] E. Kausel, Fundamental solutions in elastodynamics: a compendium, Cambridge University Press, New York, 2006.

[28] P. Galvín, A. Ordóñez, Dynamic testing of pile foundations during construction of Javalambre Astrophysical Observatory, Tech. rep., Universidad de Sevilla (2012).

[29] N. Shapiro, M. Campillo, L. Stehly, M. Ritzwoller, High-resolution surface wave tomography from ambient seismic noise, Science 307 (5715) (2005) 1615–1618.
[30] R. Clough, J. Penzien, Dynamics of structures, 3rd Edition, McGraw-Hill, New York, 1995.
[31] R. Apsel, J. Luco, Impedance functions for foundations embedded in a layered medium: an integral equation approach, Earthquake Engineering and Structural Dynamics 15 (1987) 213–231.
[32] R. Dobry, G. Gazetas, Simple method for dynamic stiffness and damping of floating pile groups, Géotechnique 38 (1988) 557–574.
[33] J.-G. Sieffert, F. Cevaer, Handbook of impedance functions. Surface foundations, Ouest Editions, Presses Académiques, Nantes, 1992.
[34] G. Mylonakis, A. Nikolaou, G. Gazetas, Soil-pile-bridge seismic interaction: kinematic and inertial effects. Part I: soft soil, Earthquake Engineering and Structural Dynamics 26 (3) (1997) 337–359.
[35] C. C. Spyrakos, Assessment of SSI on the longitudinal seismic response of short span bridges, Engineering Structures 12 (1) (1990) 60–66.
[36] A. Maravas, G. Mylonakis, D. Karabalis, Simplified discrete systems for dynamic analysis of structures on footings and piles, Soil Dynamics and Earthquake Engineering 61 (2014) 29–39.
[37] G. Gazetas, N. Makris, Dynamic pile-soil-pile interaction. Part I: Analysis of axial vibration, Earthquake Engineering and Structural Dynamics 20 (2) (1991) 115–132.
[38] N. Makris, G. Gazetas, Dynamic pile-soil-pile interaction. part ii: Lateral and seismic response, Earthquake Engineering and Structural Dynamics 21 (2) (1992) 145–162.
[39] K. Konagai, R. Ahsan, D. Maruyama, Simple expression of the dynamic stiffness of grouped piles in sway motion, Journal of Earthquake Engineering 4 (03) (2000) 355–376.
[40] G. Mylonakis, G. Gazetas, Lateral vibration and internal forces of grouped piles in layered soil, Journal of Geotechnical and Geoenvironmental Engineering, Proceedings of the ASCE 125 (1) (1999) 16–25.